J. Meas. Sci. Instrum., 2025, 16(3): 446-455. http://jmsi.publish.founderss.cn
DOI: 10.62756/jmsi.1674-8042.2025043 jmsi@nuc.edu.cn

Ultra-low-frequency broadband characteristics of radial gradient supercell seismic metamaterials

LI Lixia*, LI Yan, LIU Haixia

School of Mechatronic Engineeering, Xi'an University of Archetecture and Technology, Xi'an 710055, China

***Corresponding author:** LI Lixia (jieli_18@163.com)

Received: December 19, 2023 **Revised:** January 17, 2024 **Accepted:** January 26, 2024

Abstract: This study aims to discuss the propagation characteristics of seismic Lamb wave and surface wave in a new radial gradient supercell seismic metamaterial (RGSSM). Different from the traditional seismic metamaterials with simple unit cells, the RGSSM consists of the supercells arranged periodically along the radial direction, and these supercells are composed of five kinds of unit cells with gradient filling rates. The dispersion curve and attenuation spectrum of the Lamb wave in RGSSM are studied with the finite element method combined with the supercell technology, generating a very low-frequency ultra-wide bandgap of 3.98—20 Hz, and a forbidden band generated by the localized modes forms multi-harmonic oscillators inside the supercell. Furthermore, it is found that the Young's modulus of the soil is more sensitive to the effect of bandgap. In terms of surface wave, the RGSSM can produce rapid attenuation in the low frequency range of 5.2—8.5 Hz. Finally, a 3D model is designed to demonstrate the shielding performance of RGSSM against the seismic surface wave. The proposed RGSSM provides a new idea for the seismic isolation of ultra-wide and low-frequency seismic waves.

Key words: radial gradient supercell seismic metamaterials (RGSSM); supercellular method; ultra-low-frequency broadband

0 Introduction

Earthquake is one of the most catastrophic natural disasters. The propagation of earthquake source has caused a lot of damage to building structures[1], and further resulted in the consumption and damage of all aspects of social resources[2]. As an artificial structure that attenuates seismic waves, seismic metamaterial can generate forbidden bands corresponding to seismic frequencies, providing new ideas for building protection[3,4].

Seismic surface wave has the characteristics of large amplitude, long propagation distance and low frequency, causing great harm to buildings. For a long time, the research on seismic metamaterial has focused on the surface wave[5,6] while seismic Lamb wave has been ignored as another form of seismic wave propagation. It has been found that in the case of near-surface earthquake, the propagation of Lamb wave is a key factor to damage the buildings[7], which usually dominates the seismic records of local and regional events[8]. Therefore, when designing a seismic metamaterial, it is necessary not only to conduct seismic isolation design for surface wave, but also to study the shielding properties of Lamb wave.

Du et al.[9] studied the shielding effect of periodic concrete structure on seismic Lamb wave, determined the blocking effect of periodic structures on Lamb wave, and confirmed the existence of low-frequency bandgap, but there is a situation in which the bandgap range is narrow. Zhang et al.[10] studied the propagation of Lamb wave in seismic metamaterial with periodic arrangement of different cross-sections, and discussed the discontinuous bandgap of 6—19 Hz based on the Bragg scattering mechanism. Huang et al. [11] used auxetic foam as a new seismic metamaterial for Lamb wave. By analyzing the energy band structure and vibration mode of the upper and lower bounds of a complete bandgap, it was verified that the Lamb wave has a good attenuation effect in the frequency range below 10 Hz, but the corresponding bandgap is narrow, limiting its applications in engineering. Radial metamaterial is widely used in various fields of vibration isolation and noise reduction owing to its excellent bandgap properties and omnidirectional shielding[12-14]. Li et al.[15] introduced radial metamaterial into seismic metamaterial, and proposed a radial seismic metamaterial with wider bandgap for seismic Lamb and surface waves.

Metamaterial[16,17] with gradient structure demonstrates a wide range of tailored properties. Lin et al.[18] designed a

2D gradient-index phononic crystal, demonstraing that such a structure enables broadband acoustically focusing across a wide operating frequency range. Liang et al.[19] designed a two-dimensional omnidirectional sound absorber with a gradient-index phononic crystal as the shell, and found that sound wave can be bent by the gradient-phononic crystal shell and absorbed by the inner core in a wider range. The greatest advantage of the gradient structure is that the transmission of elastic wave can be manipulated in a wide frequency domain[20,21]. Yu et al.[22] proposed a seismic metamaterial with a gradient of buried depth, and the transmission spectrum of its finite structure shows that it has a better seismic isolation effect on surface wave in a wider bandgap. However, the dispersion curve of the gradient-arranged seismic metamaterial structure has not been calculated and studied, and the mechanism of bandgap widening has not been analyzed.

The supercell is composed of several unit cells with different parameters. The calculation of the energy band for the supercell with periodic structure is called the supercell method. Wu et al.[23] found that the supercell method is effective in studying the acoustic bandgap regarding the effect of translation group symmetry on phonon bandgap. Yuan et al.[24] utilized the sub-crystal plate to verify the characteristics of supercell structure, obtaining a wide and low-frequency bandgap by adjusting the bandgap. Young et al.[25] designed a 45° rotated supercell to achieve bandgap optimization. These methods make it possible to widen the bandgap via the periodic gradient structure of the metamaterials.

In this study, the gradient idea is applied to the design of radial seismic metamaterial, and its low-frequency broadband characteristics and mechanisms are analyzed and studied combined with the supercell method. First, the dispersion curves, transmission spectra and mode shapes of special points of five radial seismic metamaterials with different filling rates are studied. Next, the supercell of radial gradient seismic metamaterial is designed, and the formation mechanism of ultra-low-frequency ultra-wide bandgap is analyzed. Furthermore, the effects of different material parameters in the supercell on the bandgap are investigated. At last, the attenuation effect of radial gradient supercell seismic metamaterial on seismic surface wave is studied by using a three-dimension model, and the time domain verification is carried out.

1 Basic theory

The propagation of seismic wave can be described as the propagation of elastic wave in inhomogeneous media. Assuming that the seismic wave propagates along the radial midplane of the structure, the governing equation can be written as

$$\rho(r)\ddot{u}(r)=\nabla\left\{\left[\lambda(r)+2\mu(r)\right]\nabla u(r)\right\}-\nabla\times\left[\mu(r)\times u(r)\right], \tag{1}$$

where $\rho(r)$ is mass density, $u(r)$ represents the displacement vector, $\lambda(r)$ and $\mu(r)$ are the Lame constants, and ∇ is the inverted triangle operator. To study the eigenfields inside the metamaterial, the body force is assumed to be zero. Due to the particularity of the structure, Eq. (1) is extended to the elastic wave equation in the cylindrical coordinates as

$$\begin{aligned}\rho\frac{\partial^2 u}{\partial t^2}&=(\lambda+2\mu)\frac{\partial\theta_t}{\partial r}-\frac{2\mu}{r}\frac{\partial w'_z}{\partial\theta}+2\mu\frac{\partial w'_\theta}{\partial\theta'},\\ \rho\frac{\partial^2 v}{\partial t^2}&=(\lambda+2\mu)\frac{\partial\theta_t}{r\partial\theta}-2\mu\frac{\partial w'_z}{\partial\theta}+2\mu\frac{\partial w'_r}{\partial r},\\ \rho\frac{\partial^2 w}{\partial t^2}&=(\lambda+2\mu)\frac{\partial\theta_t}{\partial z}-\frac{2\mu}{r}\frac{\partial(rw'_\theta)}{\partial r}+\frac{2\mu}{r}\frac{\partial w'_r}{\partial\theta'},\end{aligned} \tag{2}$$

where u, v, and w are the displacement components in the Cartesian coordinate system, ρ is the density, t is the time, λ and μ are the elastic wave constants of the material, and r, θ, and z are the coordinates in the cylindrical coordinate system.

Furthermore, the body strain θ_t and rotation components (w'_r, w'_θ, w'_z) are defined as

$$\begin{aligned}&\theta_t=\frac{1}{r}\frac{\partial(ru)}{\partial r}+\frac{1}{r}\frac{\partial v}{\partial\theta}\frac{\partial w}{\partial z},\quad w'_r=\frac{1}{2}\left(\frac{1}{r}\frac{\partial w}{\partial\theta}+\frac{1}{r}\frac{\partial v}{\partial z}\right),\\ &w'_\theta=\frac{1}{2}\left(\frac{1}{r}\frac{\partial u}{\partial\theta}+\frac{\partial w}{\partial r}\right),\quad w'_z=\frac{1}{2}\left(\frac{1}{r}\frac{\partial(rv)}{\partial\theta}+\frac{\partial u}{\partial\theta}\right).\end{aligned} \tag{3}$$

Since the periodic structure of a lattice unit is infinite in the radial direction, according to Bloch's theorem, only a single lattice unit needs to be considered. The boundary condition of the lattice is expressed as

$$u(r+r_a,z)=u(r,z)e^{ik_r r_a}, \tag{4}$$

where r and r_a are the radial position vectors, a is the lattice constant, and k_r represents the one-dimensional Bloch radial wave vector. Herein, the Floquet periodic boundary condition is applied to the edge of unit radial, and the free boundary condition is applied to the top and bottom surfaces of unit cell simulating seismic Lamb wave, i.e. there are no reflected components on the surface[15].

2 Vibration damping properties of RGSSM on Lamb wave

2.1 Bandgap properties of unit cells

The scheduling results of scenario 1 are shown in Fig. 1. It can been seen that the unit cell of radial supercell seismic metamaterial is composed of a steel

ring embedded in the soil, and its lattice and spatial lattice structures are shown in Figs. 1(a) and (b), respectively, where the lattice constant is a, the height $b=0.5a$, the thickness of the steel ring is c, and the filling rate is defined as c/a.

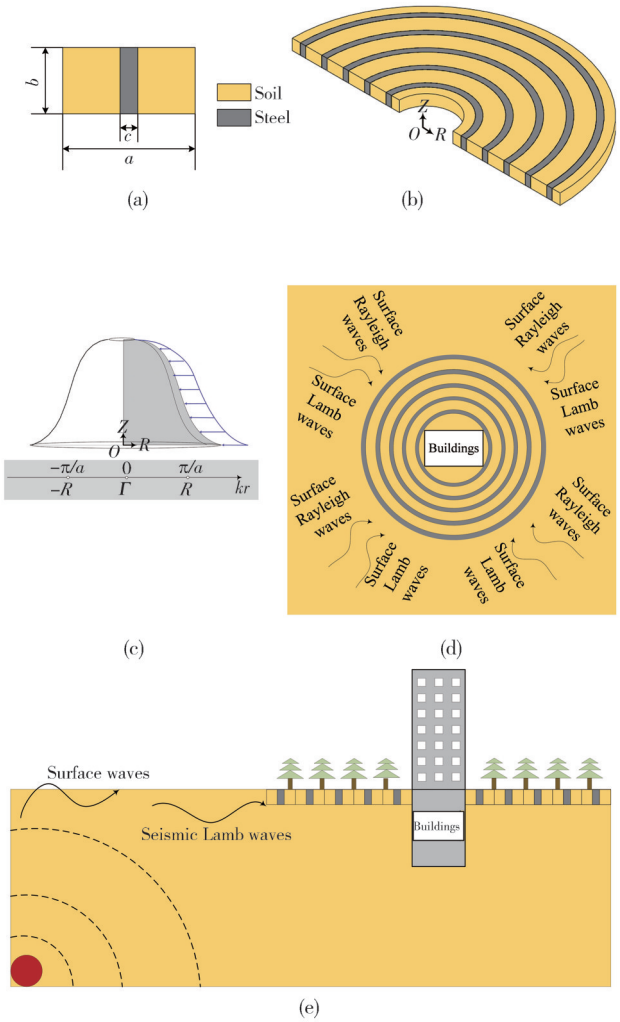

Fig. 1 Radial seismic metamaterial barrier. (a) Cross-section of radial periodic seismic metamaterial barrier, (b) 3D radial periodic seismic metamaterial barrier, (c) Berezovskii - Zakharov wave vector in reciprocal space, (d) and (e) Radial seismic metamaterial for buildings overall arranged

According to different earthquake-related geophysical survey data, the corresponding wavelengths of seismic waves vary from several meters to hundreds of meters. Therefore, for the periodic structure with lattice constant of 4 m in this study, its lattice constant is almost one-twentieth of the wavelength of seismic wave. The radial seismic metamaterial unit cell constructs a three-dimension structural model by periodically repeating the two-dimensional axisymmetric model along its radial direction and rotating around Z-axis, thereby forming an infinite system of radial seismic metamaterial. Its formation and the Berezovskii-Zakharov (BZ) wave vector in the reciprocal space are shown in Fig.1(c). The radial seismic metamaterial composed of radial periodic steel rings in the soil around the protected building is shown in Fig. 1(d). The overall arrangement of radial seismic metamaterial for buildings is shown in Fig.1(e).

To achieve high cost-effective engineering solutions, soil serves as the matrix, whereas high-strength steel, a conventional building material, acts as the scatterer within the radial seismic metamaterial. The composite system is modeled as linear-elastic, homogeneous, and isotropic, with material properties detailed in Table 1.

Table 1 Material properties

Material	Young's modulus/Pa	Density/(kg·m^{-3})	Poission's ratio
Steel	2.70×10^{11}	7 850	0.3
Soil	2.10×10^{7}	1 800	0.3

To verify the bandgap generated by the radial seismic metamaterial barrier, a 3D model as shown in Fig.2(a) is established.

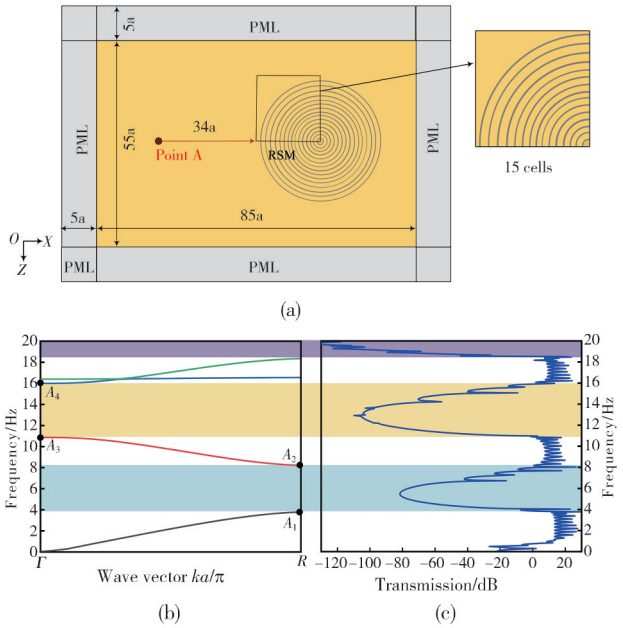

Fig. 2 Bandgap and attenuation spectrum of radial seismic metamaterial. (a) 3D model of radial seismic metamaterial barrier, (b) Dispersion curve of radial seismic metamaterials at a filling rate of 0.15, and (c) Transmission spectrum at a filling rate of 0.15

A limited number of seismic metamaterials with a filling rate of 0.15 were arranged radially, and point displacements were used to excite the Lamb wave in the soil. For the Lamb wave, the distance between the wave source and the barrier is set as 20a, and a perfectly matched layer (PML) with a width of 3a is applied around the barrier, so that the reflection of the seismic wave at the soil boundary can be eliminated to obtain more accurate results. Of course, a low-reflection boundary can achieve the same purpose. In

this study, the incident wave polarized along the Y-axis direction is used for frequency domain analysis in the ultra-low-frequency range of 0.1—20 Hz, and a tetrahedral mesh with quadratic element size of $\lambda_T/5$ (λ_T is the wavelength of the shear wave) in the finite period model is set up. The transmission is defined as $20\log(\alpha_{output}/\alpha_{input})$, where α_{output} and α_{input} are the transmission acceleration and the incident acceleration, respectively. The calculated attenuation spectrum curve of the 15-period radial seismic metamaterial is shown in Fig.2(c), which is clearly consistent with the dispersion curve in Fig.2(b).

By setting the unit cells with filling rates of 0.15, 0.25, 0.35, 0.45 and 0.55, respectively, and using Comsol Multiphysics 5.5 to calculate the Lamb wave's energy band curves of five radial seismic metamaterials with different filling rates, we can obtain the results in Fig.3. It can be seen that when the filling rate is 0.15, there are three complete bandgaps in the frequency range of 0—20 Hz: the first bandgap, 3.781 2—8.170 Hz; the second bandgap, 10.851—15.987 Hz; and the third bandgap, 18.358—20Hz. With the gradual increase of the filling rate, the starting frequency of the first bandgap remains unchanged, whereas the cut-off frequency gradually increases, thus widening the first bandgap gradually.

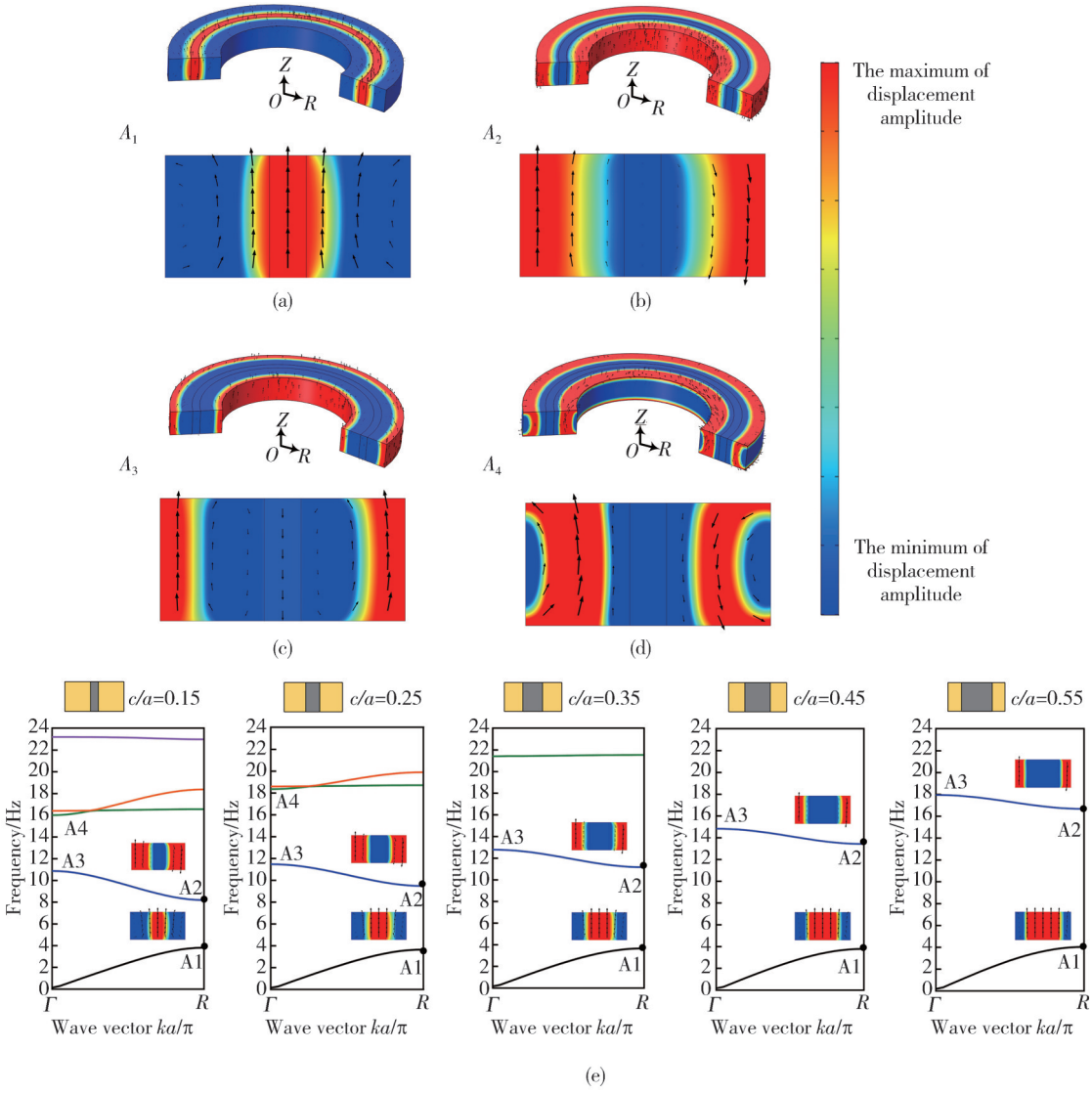

Fig. 3 Bandgap characteristics of radial seismic metamaterials with different filling rates. (a) Vibration mode at point A1, (b) Vibration mode at point A2, (c) Vibration mode at point A3, (d) Vibration mode at point A4, and (e) Dispersion curves of radial gradient supercell unit cells under different filling rates

To explore the mechanism of the bandgap, the vibration modes at special points under different filling rates are shaped, as shown in Fig. 3, where the black arrows represent the direction of the vibration displacement and the colors represent the magnitude of the vibration displacement. From the modal shape at the special point of the first bandgap under five different filling rates, it can be known that the modal shape of the first band start frequency is the vibration of the steel ring along the Z-axis direction, and the soil provides the elastic constant. For the cut-off

frequency, the vibration modes of different filling rates are the anti-phase vibration of the soil on both sides of the steel ring, and the steel ring is almost static. These two local resonance modes couple with the Lamb mode to form the first bandgap.

Observing Fig.3(e), it can also be found that with the filling rate increasing, the initial frequency of the first bandgap is almost unchanged. This is because the mass of the steel ring gradually increases with the filling rate increasing, but the reduction of soil in cross-sectional area also makes the elastic constant increase, so the onset frequency of the first bandgap does not change. In addition, as the filling rate increases, the cut-off frequency of the first bandgap moves to high frequencies, because with the increase of the filling rate, the elastic coefficient provided by the soil increases while the quality of the soil decreases instead. Consequently, the cut-off frequency of the while first bandgap moves up rapidly, so that the width of the first bandgap increases. When the fill rate is 0.55, the bandgaps within 4.006—16.661 Hz and 17.942—20 Hz can be generated in the low frequency range of 0—20 Hz.

2.2 Radial gradient supercell seismic metamaterial

In the RGSSM designed in this section, five single cells with different filling rates (0.15, 0.25, 0.35, 0.45, 0.55) are formed into the supercell, which extend periodically along the radial direction. Fig.4(a) is a two-dimensionalal cross section of the RGSSM, and the spatial lattice structure formed by rotating around the Z-axis is shown in Fig.4(b), which is periodically embedded in the soil matrix to protect the central sensitive building, as shown in Fig.4(c). The material parameters in Fig.4 are consistent with those in Table 1.

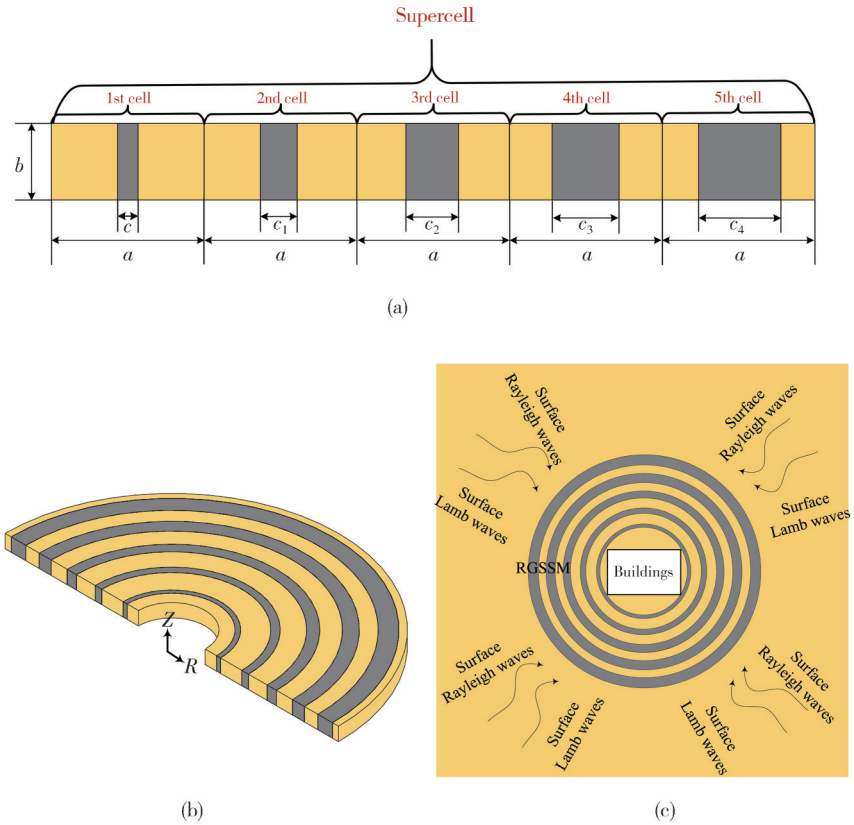

Fig. 4 Radial supercell seismic metamaterial B. (a) Two-dimensionalal cross section of RGSSM, (b) RGSSM spatial lattice structure, and (c) RGSSM, which consists of steel rings embedded in the soil gradient around the building to be protected

The energy band structure of RGSSM is calculated by using the supercell method. As there are five cells in the supercell structure, the Brillouin zone is five times as large as the original cell. The Brillouin zone boundary of radial seismic metamaterial cell range from $\Gamma(0, 0)$ to $R(1, 0)$, and the Brillouin zone boundary of RGSSM ranges from $\Gamma(0, 0)$ to $R(5, 0)$. Therefore, one energy band of a single cell is folded into five energy bands in the supercell structure, and the five energy bands in the supercell are called a group of energy bands. Fig.5(a) shows the energy band structure of RGSSM, and it can be found that it has a very low frequency ultra-wide bandgap of 3.98—20 Hz. In addition, it is observed that there are many localized flat bands in the energy band structure.

Theoretically, perfect filtering characteristics exist in

the periodic structure with infinite units, but in practical engineering applications, the number of units is always limited. In order to further verify the attenuation characteristics of the proposed RGSSM, a finite three-dimensional periodic system is simulated. The attenuation spectra of RGSSM with 1-period and 3-period finite structures are calculated respectively. As shown in Fig. 5(b), the attenuation spectrum curves of 1-period and 3-period RGSSM obviously correspond to the energy band structure of that in Fig. 5(a), while in the higher frequency range, 3-period RGSSM has better bandgap characteristics.

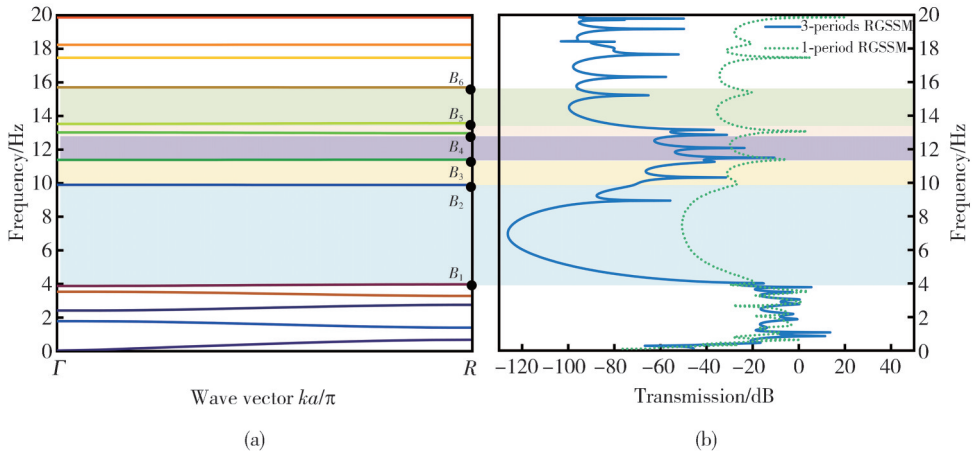

Fig. 5 Bandgap and attenuation spectrum of radial supercell seismic metamaterial. (a) Correspondence between dispersion curve and transmission spectrum curve of RGSSM, and (b) Transmission spectrum curves of 1- and 3-period RGSSMs

2.3 Mechanism analysis of ultra-low-frequency broadband

To study the generation mechanism of RGSSM bandgap, the vibration modes of RGSSM at special points $B1$, $B2$, $B3$, $B4$, $B5$ and $B6$ in Fig. 5(a) are calculated, and the results are shown in Fig.6.

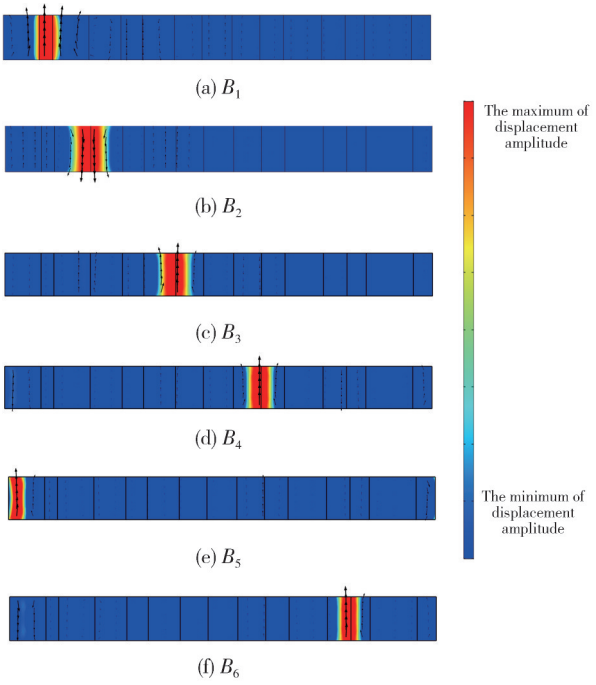

Fig. 6 Vibration modes of RGSSM at ponts *B*1, *B*2, *B*3, *B*4, *B*5, *B*6

It can be seen that the vibration mode of RGSSM at point $B1$ is concentrated in the supercell, and the steel ring of the first unit cell vibrates along the Z-axis direction, while other parts basically remain stationary. The vibration modes of RGSSM at special points $B2$, $B3$, $B4$, $B5$ and $B6$ on the flat belt are localized vibration of the soil layer along the Z-axis direction.

In order to further study the shielding effect of RGSSM on earthquake Lamb waves, the commercial finite element software COMSOL Multiphysics 5.5 was used to calculate a three-dimensional finite model composed of 3-period RGSSM, PML and soil matrix. The structural dimensions used to build the three-dimensional finite system are consistent with the parameters in Fig.4(a), and the material parameters are consistent with that in Table 1. The incident wave is applied at a distance of 140 m from the center of the barrier, and then the acceleration is collected in the protected area of the center of the barrier.

The directional displacement fields of incident waves at two frequencies inside and outside the bandgap are calculated, as shown in Fig.7(a) and (b), respectively. It can be seen that at 2.3 Hz, the radial gradient supercell barrier has almost no shielding effect on seismic waves. However, at 9.2 Hz, the seismic wave is completely reflected and isolated from the radial gradient hypercell structure barrier, and the internal protection area is not affected. This phenomenon shows that in the frequency range within the bandgap, the radial gradient supercellular seismic metamaterial can provide a safe area when seismic waves interfere.

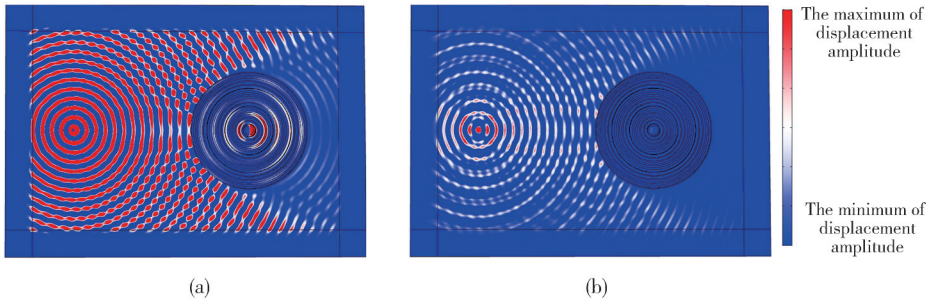

Fig. 7 Shielding effect of RGSSM on Lamb wave. (a) Shielding effect of RGSSM out of band on Lamb wave at 2.3 Hz, and (b) Shielding effect of RGSSM in bandgap on Lamb wave at 9.2 Hz

2.4 Influence of material parameters on bandgap

To further verify the bandgap mechanism of radial gradient supercell, the parameters of supercell structure are analyzed and verified. In this section, the influence of the soil connecting the first unit cell with the second unit cell on the bandgap is studied, and the dispersion curve affected by this parameter is extracted and analyzed. Generally, the Young's modulus and mass density of soil vary in the range of 1—90 MPa and 1 600—2 200 kg·m^{-3}, respectively.

It can be seen from Fig.8(a) that with the increase of Young's modulus of soil, the vibration frequencies of $B1$ and $B2$ modes gradually increase. The $B1$ mode mainly shows that the steel ring vibrates along the Z-axis, the mass density of the steel ring remains unchanged, and the soil stiffness increases, so the frequency moves to a higher frequency. Compared with the vibration frequency in $B1$ mode, the vibration in $B2$ mode is more significantly affected by the Young's modulus of soil. Compared with the influence of soil Young's modulus on vibration frequency, the influence of soil mass density is not obvious. With the increase of soil mass density, the vibration frequency of $B1$ mode has no obvious change, while the vibration frequency of $B2$ mode moves down slowly with the increase of soil mass density. This is because with the increase of soil mass density, the mass of soil between the first unit cell and the second unit cell as vibrator increases while the vibration frequency decreases.

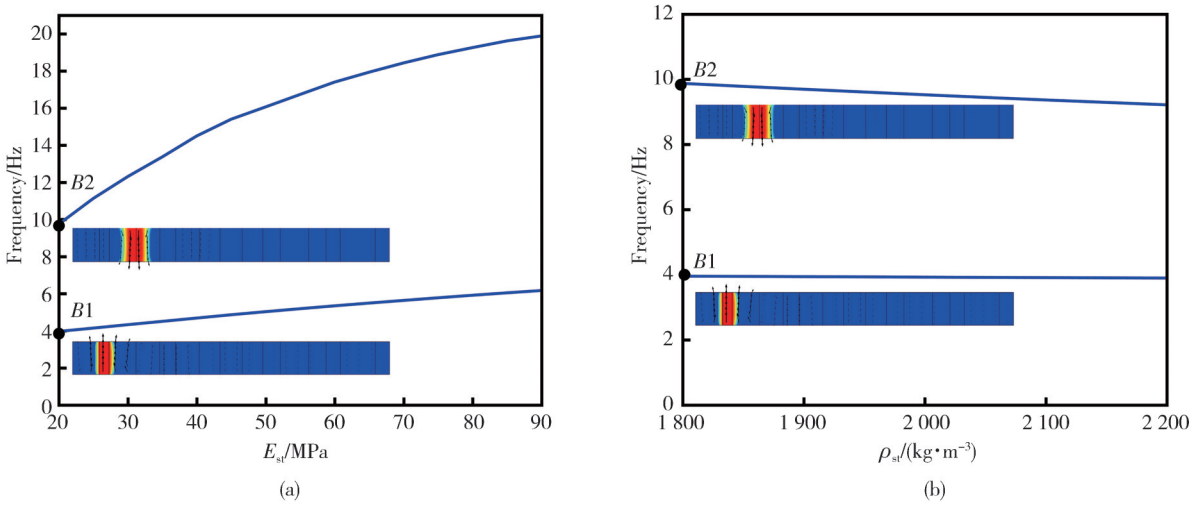

Fig. 8 Changes of vibration frequency of B1 and B2 modes with soil parameters for the connection between the first unit cell and the second unit cell. (a) Changes of vibration frequency with Young's modulus of soil, and (b) Changes of vibration frequency with soil mass density

3 Attenuation characteristics of RGSSM to surface wave

In order to study the attenuation effect of RGSSM on seismic surface waves, the surface wave transmission coefficients of RGSSM with three finite periods were calculated. As shown in Fig.9(a), the system consists of radial gradient supercellular seismic metamaterial and soil basement. Perfect matching layers are added to the left and right sides and bottom sections of the model to eliminate the influence of reflection on the research results. The material parameters used in the system are consistent with those in Table 1. A line source Line A is designed between the soil base of the model and the

perfect matching layer on the left to simulate the incident surface wave along the X-axis direction.

To further analyze the shielding effect of 3-period RGSSM composite system on seismic surface waves, the displacement field of incident wave within the bandgap is given in this subsection. The displacement field diagram of 6.7 Hz is shown in Fig. 9(c), and the displacement field of the system without RGSSM is shown in Fig. 9(d). It can be observed that when the seismic wave reaches the seismic metamaterial, obvious refraction occurs in the propagation direction of the surface wave, and part of the surface wave is converted into bulk wave, and the energy is consumed in the soil base, while part of the energy is concentrated in the steel ring.

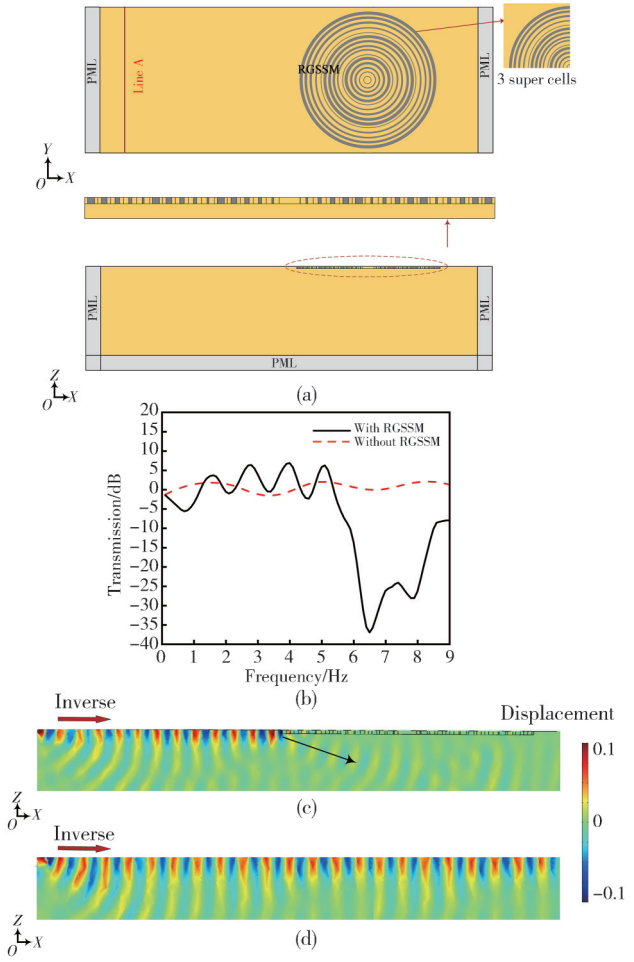

Fig. 9 Attenuation effect of RGSSM on seismic surface waves. (a) Two-dimensionalal schematic diagram of finite RGSSM system used for attenuation spectrum and time domain calculation, (b) Transmission spectrum curve of seismic surface wave passing through the barrier with and without RGSSM, (c) Displacement diagram of 3-period RGSSM, and (d) Displacement diagram of non-seismic metamaterial (−0.1 and 0.1 present the minimum and the maximum of displacement amplitude, respectively)

To further verify the attenuation effect of RGSSM on surface waves, the acceleration-time response of RGSSM under the action of EI-Centro surface waves was studied. Theoretically, perfect filtering characteristics exist in the periodic structure with infinite cells. However, in practical engineering applications, the number of units is always limited. To further verify the effectiveness of response surface model in reducing seismic surface waves, a three-dimensional 3-period RGSSM system is used for numerical simulation. The representative EI-Centro seismic wave is selected for analysis. Fig. 10(a) and (b) show the acceleration time history of EI Centro wave and the frequency spectrum curve of seismic wave, respectively. Fig.10(c) and (d) show the acceleration responses of the periodic barrier in the X- and Z-axis directions caused by the EI-Centro seismic wave as the seismic source, respectively. It can be seen that the periodic barrier has obvious effect on the attenuation of seismic waves in the bandgap range, and its attenuation amplitude obviously exceeds 70% especially in the X-axis direction. This result proves that the RGSSM has certain attenuation effect on seismic waves in the bandgap range, thus avoiding the building structure from being invaded by seismic waves in all directions.

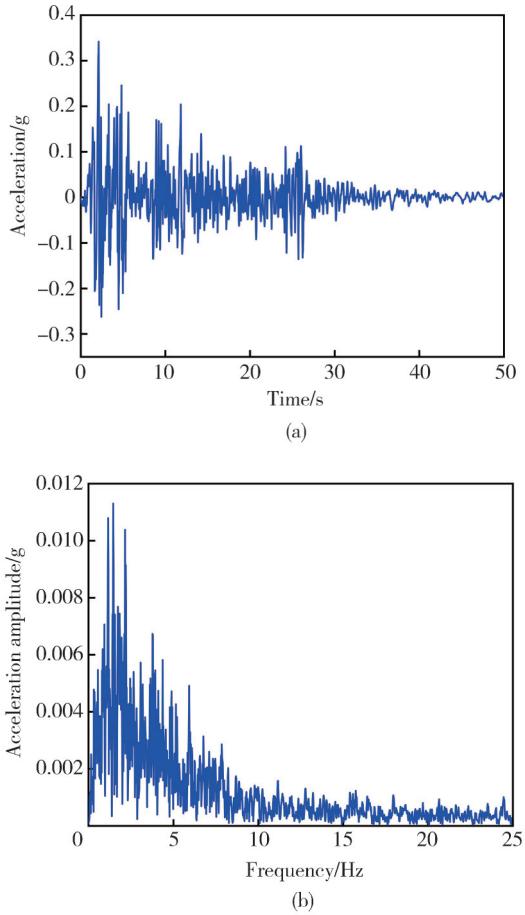

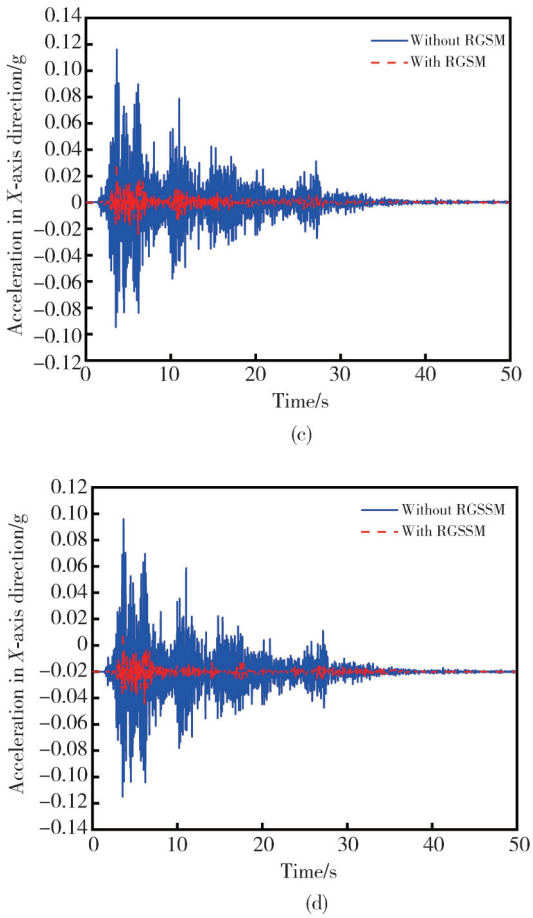

Fig. 10 Acceleration response with EI-Centro seismic waves. (a) Time history diagram of EI - Centro seismic wave, (b) EI-Centro seismic wave spectrum curve, (c) x-asix direction acceleration response, and (d) z-axis direction acceleration response

4 Conclusions

To sum up, an RGSSM is proposed to attenuate seismic Lamb wave and surface wave. The dispersion curve and vibration modes of special points are calculated by finite element method, the generation mechanism of bandgap is analyzed, the influence of material parameters on bandgap is discussed, and a three-dimensional model is established to calculate the transmission spectrum for verification. Similarly, the attenuation effect of RGSSM on seismic surface waves is calculated, and finally it is verified in time domain. The research shows that the RGSSM has an ultra-wideband damping effect on Lamb waves below 20 Hz, and the attenuation range is 3.98—20 Hz. The widening of the bandgap is due to the periodic gradient arrangement of filling rate, which introduces local resonators with different masses, and the flat band in the corresponding frequency range opens the bandgap. For soil mass density, the influence of soil Young's modulus on the bandgap is more significant. With the increase of soil Young's modulus, the bandgap widens significantly and moves to high frequency. On the contrary, with the increase of soil density, the bandgap narrows slowly. Then, it is verified that the RGSSM has a good shielding effect on seismic Lamb waves in the bandgap range. It can also effectively attenuate the seismic surface wave from 5.2 Hz to 8.5 Hz. The common building materials, soil and steel used in the above structures have high performance and low cost, thus realizing the seismic wave shielding. This work develops and perfects the existing field of seismic metamaterials, and provides a novel design guide for civil engineers to design seismic metamaterials.

Acknowledgement

I would like to express my gratitude to the reviewers and editors.

Declaration of conflicting interests

The authors have no conflict of interests related to this publication. The authors have no conflict of interests related to this publication.

References

[1] ACHAOUI Y, ANTONAKAKIS T, BRÛLÉ S, et al. Clamped seismic metamaterials: ultra-low frequency stop bands. New Journal of Physics, 2017, 19(6): 063022.

[2] ACHAOUI Y, UNGUREANU B, ENOCH S, et al. Seismic waves damping with arrays of inertial resonators. Extreme Mechanics Letters, 2016, 8: 30-37.

[3] COLOMBI A, COLQUITT D, ROUX P, et al. A seismic metamaterial: The resonant metawedge. Scientific Reports, 2016, 6: 27717.

[4] KRÖDEL S, THOMÉ N, DARAIO C. Wide band-gap seismic metastructures. Extreme Mechanics Letters, 2015, 4: 111-117.

[5] DU Q J, ZENG Y, XU Y, et al. H-fractal seismic metamaterial with broadband low-frequency bandgaps. Journal of Physics D Applied Physics, 2018, 51(10): 105104.

[6] COLOMBI A, ROUX P, GUENNEAU S, et al. Forests as a natural seismic metamaterial: Rayleigh wave bandgaps induced by local resonances. Scientific Reports, 2016, 6: 19238.

[7] BORMANN P, ENGDAHL B, KIND R. Seismic Wave Propagation and Earth Models. New Manual of Seismological Observatory Practice 2, 2012, 2: 1-80.

[8] PARK C B, RYDEN N, WESTERHOFF R, et al. Lamb waves observed during MASW surveys. SEG Technical Program Expanded Abstracts, 1999, 21(1):1400.

[9] DU Q J, ZENG Y, HUANG G L, et al. Elastic

metamaterial-based seismic shield for both Lamb and surface waves. AIP Advances, 2017, 7(7): 075015.
[10] ZHANG K, LUO J, HONG F, et al. Seismic metamaterials with cross-like and square steel sections for low-frequency wide bandgaps. Engineering Structures, 2021, 232: 111870.
[11] HUANG T T, REN X, ZENG Y, et al. Based on auxetic foam: a novel type of seismic metamaterial for Lamb waves. Engineering Structures, 2021, 246: 112976.
[12] CHEN M J, WANG C X, CHENG X D, et al. Experimental demonstration of invisible electromagnetic impedance matching cylindrical transformation optics cloak shell. Journal of Optics, 2018, 20(4): 045608.
[13] WU X Y, HU C G, WANG M, et al. Realization of low-scattering metamaterial shell based on cylindrical wave expanding theory. Optics Express, 2015, 23(8): 10396.
[14] MA T, CHEN T N, WANG X P, et al. Band structures of bilayer radial phononic crystal plate with crystal gliding. Journal of Applied Physics, 2014, 116(10): 104505.
[15] LI L X, JIA Q, TONG M J, et al. Radial seismic metamaterials with ultra-low frequency broadband characteristics. Journal of Physics D: Applied Physics, 2021, 54(50): 505104.
[16] LU K, TIAN Y J, GAO N S, et al. Propagation of longitudinal waves in the broadband hybrid mechanism gradient elastic metamaterials rods. Applied Acoustics, 2021, 171: 107571.
[17] ZHAO J F, MARCHAL R, BONELLO B, et al. Efficient focalization of antisymmetric Lamb waves in gradient-index phononic crystal plates. Applied Physics Letter, 2012, 101(26): 261905.
[18] LIN S, HUANG T J, SUN J H, et al. Gradient-index phononic crystals. Physical Review, B: Condensed Matter and Materials Physics, 2009, 79(9): 185502-185506.
[19] LIANG Y J, CHEN L W, WANG C C, et al. An acoustic absorber implemented by graded index phononic crystals. Journal of Applied Physics, 2014, 115(24): 244513.
[20] TORRENT D, SÁNCHEZ-DEHESA J. Acoustic metamaterials for new two-dimensionalal sonic devices. New Journal of Physics, 2007, 9(9): 323.
[21] LIN S S, HUANG T J, SUN J H, et al. Gradient-index phononic crystals. Physical Review B: Condensed Matter and Materials Physics, 2009, 79(9): 094302.
[22] LIU Z, QIN K Q, YU G L. Partially embedded gradient metabarrier: broadband shielding from seismic Rayleigh waves at ultralow frequencies. Journal of Engineering Mechanics, 2020, 146(5): 04020032.
[23] MU Z F, WU F G, ZHANG X, et al. Effect of translation group symmetry on phononic bandgaps studied by supercell calculation. Acta Physica Sinica, 2007, 56(8): 4694.
[24] YUAN L L, ZHAO P, DING Y, et al. Study on lamb waves in a composite phononic crystal plate. Crystals, 2020, 10(9): 799.
[25] AHN Y K, OH J H, MA P S, et al. Dispersion analysis with 45°-rotated augmented supercells and applications in phononic crystal design. Wave Motion, 2016, 61: 63-72.

径向梯度超元胞地震超材料的甚低频超宽带的减振特性

李丽霞*, 黎　妍, 刘海霞

西安建筑科技大学 机电工程学院, 陕西 西安 710055

摘　要： 针对地震兰姆(Lamb)波和面波在一种新型径向梯度超元胞地震超材料(Radial gradient supercell seismic metamaterial, RGSSM)中的传播特性进行了研究。与传统地震超材料的简单单胞不同, RGSSM由超元胞沿径向呈周期性排列构成, 其超元胞由五种填充率呈梯度的单胞组成。采用有限元法结合超元胞技术研究Lamb波在RGSSM中的色散曲线和衰减谱, 发现有3.98—20 Hz的甚低频超宽禁带生成。对特殊点的模态振型分析显示, 超宽禁带由超元胞内部形成多谐振子的局域化模态产生。进一步研究显示, 土壤的杨氏模量对带隙效应更加敏感。对于表面波而言, RGSSM在5.2—8.5 Hz的低频范围内对Lamb波和表面波可产生良好的衰减效果。最后, 采用设计的三维模型展示了RGSSM对地震表面波的屏蔽性能。本研究所提出的RGSSM可为超宽低频的地震波隔振提供新思路。

关键词： 径向梯度超元胞地震超材料; 超元胞法; 低频宽带

引用格式： LI Lixia, LI Yan, LIU Haixia. Ultra-low-frequency broadband characteristics of radial gradient supercell seismic metamaterials. Journal of Measurement Science and Instrumentation, 2025, 16(3): 446-455. DOI: 10.62756/jmsi.1674-8042.2025043